

Effect of groundwater flow dimensionality on mass transfer from entrapped nonaqueous phase liquid contaminants

Tarek Saba and Tissa H. Illangasekare

Division of Environmental Science and Engineering, Colorado School of Mines, Golden

Abstract. Mass transfer from entrapped nonaqueous phase liquids (NAPLs) at subsurface locations of environmental contamination typically takes place in three-dimensional groundwater flow fields. Yet most laboratory studies of NAPLs dissolution have been one-dimensional, eliminating more realistic conditions such as the heterogeneous distribution of entrapped NAPL ganglia and the potential for flow bypassing due to reduced water permeability in contaminated zones. In this study, experiments in two-dimensional flow fields were used to evaluate the effects of flow dimensionality on NAPL dissolution. Modifications of the transport code MT3D provided the capability to simulate NAPL dissolution. Regression analysis, matching experimental observations to simulated predictions, provided parameter values for a proposed phenomenological model of dissolution in two-dimensional flow fields. The proposed model predicted lower NAPL dissolution rates relative to models developed on the basis of published one-dimensional experimental measurements. The results indicate potential for significant errors using the one-dimensionally based models for NAPL dissolution in field applications.

1. Background

1.1. Introduction

The accidental release or improper disposal of petroleum products and volatile organic solvents into the subsurface have resulted in considerable subsurface contamination and created situations that potentially threaten groundwater. Processes involving the migration and entrapment of nonaqueous phase liquids (NAPLs) within the subsurface have been described by a number of authors [e.g., Pankow and Cherry, 1996]. The complex NAPL entrapment distributions resulting from soil heterogeneities have been demonstrated in cases of both lighter than and heavier than water NAPLs [Illangasekare *et al.*, 1995a, b; Held and Illangasekare, 1995]. In evaluating the potential of entrapped NAPL sources to contaminate groundwater or in designing remediation schemes, it is necessary to know the rates at which NAPLs dissolve into the flowing groundwater. Understanding the kinetics of mass transfer processes under two-dimensional flow fields is the primary focus of this paper.

1.2. Representation of Mass Transfer

A concept implicit to most mass transfer constructs is that the rate of interphase transfer is a function of a driving force and an interfacial area between the two phases of concern [Miller *et al.*, 1990]. A commonly used form of the mass transfer relationship is

$$J = k_{la} a_{na} (C_s - C) = K(C_s - C), \quad (1)$$

where J [$M L^{-3} T^{-1}$] is the solute mass flux from the immiscible liquid phase to an aqueous phase, K [T^{-1}] is a lumped mass transfer coefficient ($K = k_{la} a_{na}$), k_{la} [$L T^{-1}$] is an average mass transfer coefficient for the NAPL-water inter-

face, a_{na} is the specific interfacial area [$L^2 L^{-3}$] between entrapped NAPL and groundwater for a representative elementary volume (REV), C_s [$M L^{-3}$] is the aqueous phase concentration that corresponds to the condition of thermodynamic equilibrium with the immiscible phase, and C [$M L^{-3}$] is the solute concentration in the bulk aqueous phase. Although (1) may be suitable for estimating the general behavior of typical NAPLs, explicit mass transfer expressions relevant for specific subsurface systems are generally unavailable.

The estimation of NAPL-water interfacial contact area as well as shape and size characteristics of NAPL blobs in two-dimensional systems have been studied extensively using micromodels with etched glass. Interfacial contact area was found to be a function of pore geometry (including pore body to throat ratio, pore topology, and distribution of neighboring pore sizes), interfacial tension, wettability, viscosity, and density [Conrad *et al.*, 1987, 1989]. However, because of the complexity of entrapment configurations in naturally heterogeneous aquifers it is difficult to quantify the actual contact area between groundwater and NAPL bodies, either experimentally or mathematically [Pfannkuch, 1984; Saripalli *et al.*, 1997].

Recently, researchers have avoided the need to quantify entrapped NAPL geometry by using a lumped mass transfer coefficient K , defined as the product of the interfacial area between the NAPL and groundwater phases (a_{na}), and an average mass transfer coefficient for the NAPL-water surface (k_{la}) [Miller *et al.*, 1990; Powers *et al.*, 1992, 1994]. With the derivation of (1) the value of K , incorporating the unspecified specific surface area between phases, is determined from laboratory measurements. Methods to determine values of K are based on correlations containing a modified Sherwood number ($Sh = K d_p^2 D_m^{-1}$), where Sh is the Sherwood number, d_p (L) is the mean particle diameter, and D_m [$L^2 T^{-1}$] is the molecular diffusion coefficient for the soluble constituent [Miller *et al.*, 1990]. Table 1 provides a review of some of the dimensionless correlations used to describe interphase mass transfer.

Copyright 2000 by the American Geophysical Union.

Paper number 1999WR900322.
0043-1397/00/1999WR900322\$09.00

Table 1. Dimensionless Correlations for Interphase Mass Transfer

System	Correlation	Range	Reference
1-D NAPL	$Sh = 12 Re^{0.75} \theta_n^{0.60} Sc^{0.5}$	$0.001 < Re < 0.1$	Miller et al. [1990]
1-D NAPL	$Sh = 57.7 Re^{0.61} d_{50}^{0.64} U_i^{0.41}$	$0.01 < Re < 1$	Powers et al. [1992]
1-D NAPL	$Sh = 340 \theta_n^{0.87} Re^{0.71} (d_{50}/x)^{0.31}$	$0.0012 < Re < 0.021$	Imhoff et al. [1994]
1-D NAPL	$Sh = 4.13 Re^{0.598} \delta^{0.673} U_i^{0.369} (\theta_n/\theta_{no})^\psi$	$0.015 < Re < 0.23$	Powers et al. [1994]

Definitions of terms and variables are as follows: 1-D, one-dimensional; d_{50} , mean particle diameter [L]; Re , Reynolds number; Sh , Sherwood number; Sc , Schmidt number; U_i , uniformity index of the porous media; θ_n , volumetric content of the NAPL; θ_{no} , initial volumetric NAPL content; x , distance from the dissolution cell entrance for Imhoff et al. [1994]; δ , normalized grain size ($= d_{50}/0.05$ cm); ψ , fitting parameter which can be correlated to grain size distribution. Parameters ($\beta = 0.518 + 0.114\delta + 0.1U$) are from Powers et al. [1994].

Although these correlations developed from one-dimensional experiments offer certain capabilities for predicting NAPL dissolution process, the hypothesized exclusion of flow dimensionality will likely affect the accuracy of these relationships when applied to complex field situations. Previous work has clearly demonstrated the dramatic change in aqueous phase relative permeabilities in response to NAPL entrapment [Compos, 1998]. This phenomenon results in multidimensional flow fields that change with time during entrapped NAPLs dissolution. It is expected that the aqueous phase flow patterns affected by relative permeability changes to the flowing aqueous phase will impact the mass transfer from entrapped NAPL to groundwater. The lack of experimental data from such systems provided the motivation herein to conduct a set of two-dimensional dissolution experiments investigating the effects of flow field dimensionality, relative permeability, and groundwater velocity on NAPL dissolution. To that end, in this study we evaluated the applicability of existing correlations of the lumped mass transfer coefficient estimations for two-dimensional flow experiments and demonstrated, through intermediate-scale laboratory tests, improvements of a proposed phenomenological dissolution model allowing for flow dimensionality over existing models.

2. Experimental Design

2.1. Soil Flume

Dissolution experiments were conducted in a two-dimensional intermediate-scale soil flume. The flume was made of Plexiglas and steel, with dimensions of 2.2 m × 1.1 m × 5.08

cm (length × height × width). Two constant head supply tanks, with connections to the end of the flume, were used to create certain water table configurations and hydraulic gradients. The supply tanks could be raised or lowered during an experiment to simulate various hydraulic gradients. Figure 1 is a schematic diagram of the soil flume system.

2.2. Materials

2.2.1. Sand. Test sand with mesh size designation #30 was obtained from the Unimim Corporation (Emmet, Idaho). This sand was free of organic material or clay. In general, the sand was highly uniform and angular. Mean grain size was obtained by sieve analysis following standard American Society for Testing and Materials (ASTM) methods. Table 2 presents the physical characteristics of the sand.

Simulation of the dissolution process required the identification of the saturated hydraulic conductivity and the water relative permeability curve. The saturated hydraulic conductivity and the parameters of the Brooks-Corey [Brooks and Corey, 1964] relationship for capillary pressure versus saturation were obtained using the flow pump technique [Znidarcic et al., 1991] and are provided in Table 2. For this technique the soil sample was packed in a triaxial cell with a flexible rubber membrane wall. External pressure was applied on the triaxial cell to maintain its cylindrical shape. Saturated hydraulic conductivity of #30 sand was measured by pumping a known flow rate, using a precision flow pump, through the water-saturated soil sample, while pressure drop across the sample was measured using a pressure transducer and thereby allowing for the determination of the hydraulic conductivity. To measure the

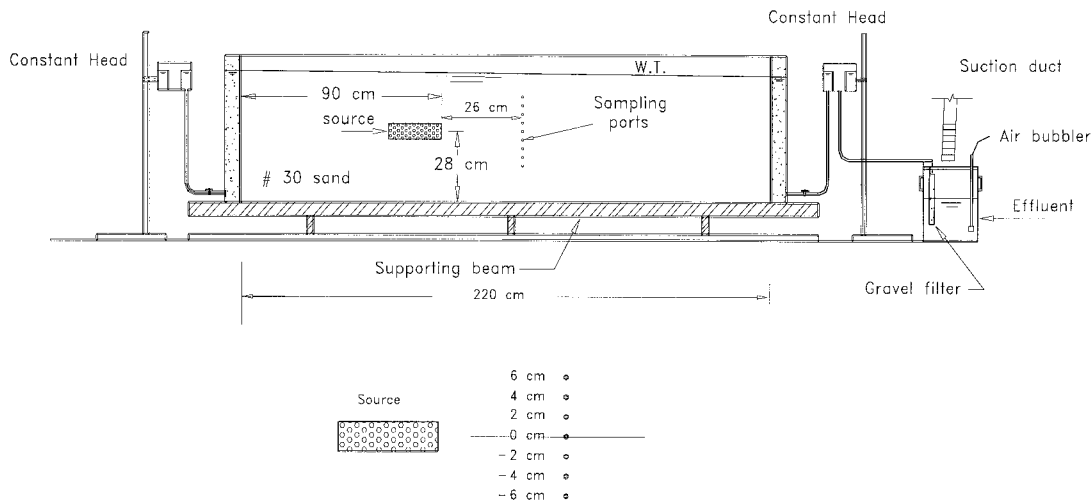


Figure 1. Schematic diagram of the experimental facility.

capillary pressure-saturation curve, the flow pump was used to control and measure the soil sample saturation, while the pressure drop across the sample was monitored continuously [Znidarcic *et al.*, 1991; Wildenschild *et al.*, 1997]. The relative permeability reductions for water were determined using the Brooks and Corey [1964] relation

$$k_{rw} = S_e^\varepsilon \quad (2)$$

where k_{rw} is the relative permeability and S_e is the effective water saturation equal to $(S - S_r)/(1 - S_r)$. S is the water saturation, S_r is the residual water saturation, ε is an empirical constant equal to $(2 + 3\lambda)/\lambda$, and λ is an index of the pore size distribution.

Wyllie [1962] used an alternate expression for the relative permeability of sand due to entrapped NAPL (xylene):

$$k_{rw} = [(1 - S_n - S_r)/(1 - S_r)]^3 \quad (3)$$

where S_n is the entrapped NAPL saturation. Demond [1988] compared three different correlations to relative permeability data collected for a sand medium saturated with water and xylene and found that Wyllie's equation described the data best. Geller and Hunt [1993] also selected Wyllie's equation to analyze their data. Equation (3) was found herein to agree with the relative permeability curve obtained from the flow pump technique using sand medium saturated with water and air; see Figure 2. In this study, Wyllie's equation was used in the estimation of relative permeability reductions due to entrapped NAPL.

2.2.2. Light nonaqueous phase test fluid. To eliminate potential experimental and interpretive complications arising because of the effects of variable compositions, a single-component NAPL (para-xylene) was used in this research. This single species, lighter than water NAPL (LNAPL), which is only slightly soluble in the aqueous phase, was assumed to negligibly affect flowing water density and viscosity due to dissolution processes. Chemical properties of para-xylene (purchased from Aldrich Chemical) are listed in Table 3.

3. Dissolution Experiments

A series of experiments were conducted in which a contaminated zone was entrapped in a two-dimensional flow field. Aqueous samples were taken downstream of the entrapped LNAPL zone at 2 cm vertical intervals (Figure 1). Break-through curves were analyzed to estimate the rate of mass depleted from the contaminated zone. LNAPL zones with different lengths, for different dissolution experiments, were prepared outside the flume so that entrapped LNAPL saturation and soil porosity could be estimated for modeling purposes.

Table 2. Measured Physical Characteristics of Sand Used

Sand Characteristic	Value for #30 Sand
Hydraulic conductivity, cm min^{-1}	7.1
Mean grain size d_{50} , cm	0.049
Brooks and Corey [1964] entry pressure, cm (of water)	5.5
Brooks and Corey [1964] pore index	2.1
Residual water saturation	0.18

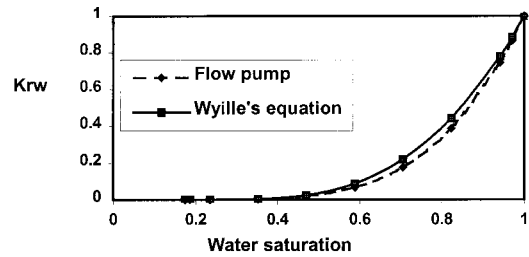


Figure 2. Relative permeability curves for #30 sand.

3.1. Source Creation

An aluminum mold with internal dimensions of 20 cm \times 5.08 cm \times 5.08 cm (height \times length \times width) was used to create LNAPL sources. Internal mold walls were covered with gaskets coated with a very thin layer of silicon grease to reduce wall effects. A peristaltic pump was used to control water flow through the mold. The mold end plates were lined with stainless steel screens and paper filters to retain the sand and distribute the LNAPL over the entire cross section when injected in a downward flow mode. The mold was initially filled with de-aired water and wet packed with test sand. A metal rod was forced into the sand to aid in settling and to break up any microlayering that might develop between lifts. To achieve complete water saturation of the sand, suction was applied at the top of the mold, while constant water head was maintained at the bottom. Two pore volumes of water were allowed to pass through the mold to wash out the fines and insure complete water saturation. On the basis of a specific gravity of sand of 2.65 g cm^{-3} , the weight of the dry sand packed in the mold, and the dry and saturated weight of the packed mold, average porosity of #30 sand packed in the mold was calculated to be 0.40.

After achieving mold saturation, para-xylene was then pumped into the mold from the top at a rate of 5 mL min^{-1} to maintain a stable front for displacement of water. Pumping of para-xylene continued until free-phase LNAPL appeared in the effluent. Following this procedure, LNAPL saturation was calculated by measuring the volume of water displaced from the mold. The saturation of para-xylene was found to be 0.85.

In order to displace potentially mobile LNAPL and any unstable globules, two pore volumes of de-aired water were then pumped into the mold at a low rate of 4 mL min^{-1} in an upward flow mode. Water injection was continued until the LNAPL was no longer displaced. This was verified by visual observation of the effluent from the mold. Water flow to the mold was then increased to 6.3 mL min^{-1} for one pore volume to obtain a minimum residual saturation by water flooding the

Table 3. Chemical Characteristics of Test LNAPL

LNAPL Characteristic	Value
Molecular formula	$\text{C}_6\text{H}_4(\text{CH}_3)_2$
Molecular weight	106.2
Melting point, $^\circ\text{C}$	13.2
Boiling point, $^\circ\text{C}$	138
Density, g cm^{-3} (at 20 $^\circ\text{C}$)	0.8611
Viscosity, cP (at 20 $^\circ\text{C}$)	0.648
Water solubility, mg L^{-1} (at 25 $^\circ\text{C}$)	156
Vapor pressure, mm Hg (at 25 $^\circ\text{C}$)	8.7
Diffusivity, $\text{cm}^2 \text{s}^{-1}$	7.2×10^{-6}

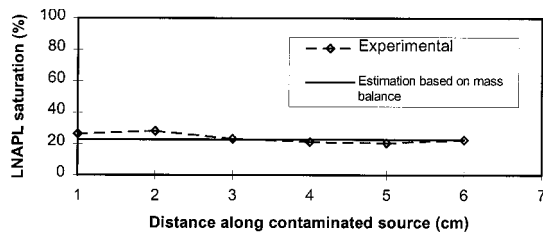


Figure 3. Light nonaqueous phase liquid (LNAPL) saturation distribution along the length of the contaminated source.

mold. The volume-averaged residual saturation was volumetrically calculated at 0.22. The mold was stored in a freezer at a temperature of -5°C to freeze the water-saturated sand containing the LNAPL entrapped at residual saturation.

To test whether or not the entrapped LNAPL was homogeneously distributed along the prepared source, the first source constructed using this method was evaluated using ultraviolet spectroscopy. The frozen source was cut into six equal pieces and placed in closable containers, and known amounts of methanol were added to the pieces to extract the para-xylene entrapped in the sand. Ultraviolet scanning at a wavelength of 254 nm was used to determine the concentration of the para-xylene in the methanol, and hence the saturation in each piece was determined. The measured LNAPL saturation along the length of the source was more or less the same as the volumetric average (Figure 3), indicating that the procedures successfully produced a contaminated source with a relatively homogeneous LNAPL saturation. This method of source creation was used to prepare all LNAPL sources used in the dissolution experiments.

3.2. Two-Dimensional Dissolution Experiments

The next phase of experiments involved placing the LNAPL source within the two-dimensional soil flume. The soil flume was wet-packed with #30 sand in 2 cm lifts under 5 cm of water. The water level was held to only a 5 cm depth to avoid significant grain size separation as the sand fell through the water. The water table was then raised by 5 cm depth increments, and the entire process was repeated until the flume was packed to the level where the frozen source was to be placed. The tank walls were locally cooled below freezing point at the source location using dry ice, and the externally prepared frozen LNAPL source was then placed on top of the packed sand in the soil flume. A very thin layer of silicon grease was applied to the acrylic walls surrounding the source to eliminate wall effects. Sand packing was continued around and on top of the source until the soil flume was completely filled with sand. The water table was then adjusted through the supply tanks at the ends of the flume to achieve the desired hydraulic gradient and thus the desired groundwater velocity.

Concentrations of dissolved para-xylene in the aqueous phase samples were measured by direct aqueous injection into a HP 5890 Series II gas chromatograph (GC) equipped with a flame ionization detector (FID). Chromatographs were integrated with a HP 3396 Series II integrator. Vertical concentration profiles were obtained once steady state dissolution was reached. The term "steady state" in this study refers to the achievement of pseudosteady concentrations at the observation ports. True steady state was not achievable because the LNAPL source was continuously being depleted (by dissolution) with time, thus changing the internal surface area be-

tween the LNAPL and water. However, because of the very low solubility of para-xylene it was expected that the changes in LNAPL saturations were negligible during the time frame of the experiment.

Once downstream pseudosteady concentrations were obtained from the sampling arrays, the flow velocity was set to a different value and another sample set was obtained. This process was repeated to detect dissolution rates over a range of hydraulic gradients. Flow rates through the tank were measured by timing the discharge of the effluent from the end reservoir.

4. Experimental Results

Following a tracer test to determine media dispersivity, natural dissolution behavior under different groundwater velocities and entrapped source lengths was investigated. Dissolution of three different source lengths was evaluated (5.08, 10.15, and 15.24 cm) in the intermediate-scale tank in separate experiments. Concentration profiles were measured downstream of the entrapped LNAPL source under several groundwater velocities ranging between 0.25 and 3.00 m d^{-1} for each source length.

4.1. Dispersivity Measurements

A tracer test was performed to determine the longitudinal and transverse dispersivity of #30 sand used for the dissolution experiments. Distilled water with para-xylene at aqueous solubility was injected in the two-dimensional soil flume containing water-saturated porous media. Numerical simulations of the tracer experiment were conducted where the dispersivities of the sand were iterated until numerical and experimental breakthrough curves matched. The iterated value of longitudinal dispersivity was found to be 0.1 cm, and the ratio between transversal to longitudinal dispersivities was found to be 0.1. These values matched previous measurements for a similar sand [Szlag, 1998].

4.2. Dissolution Fingering

In the dissolution experiments performed, the flowing aqueous phase appeared to infiltrate through the contaminated zones as multiple fingers rather than a uniform front. For example, the measured pseudosteady vertical concentration profile for the 10.16 cm source length at an aqueous velocity of 0.36 m d^{-1} is presented in Figure 4. It was expected that the

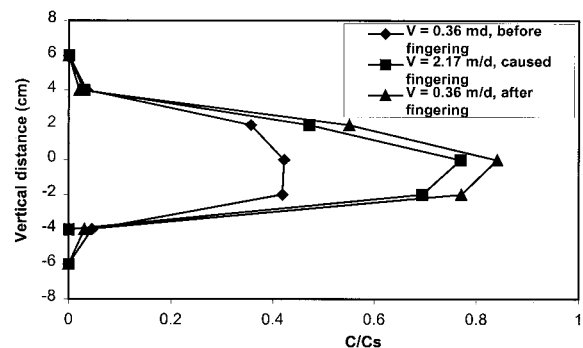


Figure 4. Transversal concentration profiles as a function of the vertical distance from the center of the LNAPL source zone. LNAPL saturation is 0.22, and source length is 10.16 cm (C_s is the solubility limit of para-xylene in water).

dissolved concentration values of the LNAPL in the flowing aqueous phase would decrease with increasing aqueous phase velocity (kinetic behavior), but this was not the case. When the average groundwater velocity was increased to 2.17 m d^{-1} , dissolved LNAPL concentration values increased. This behavior is possibly attributed to fingering of the flowing aqueous phase through the contaminated zone, a concept introduced by *Imhoff et al.* [1996] and *Imhoff and Miller* [1996].

Imhoff et al. [1996] and *Imhoff and Miller* [1996] suggest that aqueous phase may finger through a porous medium contaminated with NAPL at residual saturations. The porous medium structure and small local residual NAPL saturations influence the locations of developing fingers. In the dissolution experiment presented in Figure 4, groundwater might have infiltrated through the residually saturated zones as fingers rather than a uniform front due to local heterogeneities in the contaminated zone. By increasing groundwater velocity from 0.36 to 2.17 m d^{-1} the aqueous phase built up more pressure head to penetrate through the LNAPL zone as multiple fingers. Fingering of the aqueous phase through the contaminated zone caused an increase in the contact area between the entrapped LNAPL and groundwater, which resulted in more mass transfer and higher values for the vertical transverse concentrations. When groundwater velocity was decreased to 0.36 m d^{-1} (Figure 4), the increased contact area that resulted from the 2.17 m d^{-1} velocity remained the same. With the same contact area between entrapped LNAPL and flowing aqueous phase, the concentration values for the velocity 0.36 m d^{-1} caused higher values of transverse concentration profiles than the 2.17 m d^{-1} velocity, and dissolution behaved kinetically.

5. Phenomenological Model Development

Mass transfer is inherently a system-specific phenomenon. A convenient method of generalizing experimental data is to present them in a dimensionless form and correlate the ratios of forces affecting the system, so that a system at a different scale but with the same force ratios is expected to produce similar results. To identify the forces affecting dissolution in this study, the porous media was idealized as a bundle of tubes where the entrapped LNAPL exchanges dissolved mass with the flowing aqueous phase at the walls of these tubes. This dissolution problem can be described by a differential equation whose dimensionless solution is [Bird, 1960]

$$Sh = f [Re, Sc, (D/L^*)], \quad (4)$$

where Sh is the Sherwood number defined as $Sh = K(d_p)^2 D_m^{-1}$, Re is the average Reynolds number along the contaminated source zone given by $Re = DU\gamma^{-1}$, D [L] is the tube diameter, U [$L T^{-1}$] is the flowing aqueous phase velocity, γ [$L^2 T^{-1}$] is the kinematic viscosity of water, Sc is Schmidt number given by $Sc = \gamma/D_m$, and L^* is the tube length [L]. This analogy assumes a low rate of mass transfer and no chemical reactions in the fluid.

Since entrapped LNAPL dissolution is transient in nature, the soil pore geometry, corresponding to the tube geometry in the previous analysis, changes with time. This means that a representative of LNAPL mass change will contribute to a transient description of soil pore geometry. The dimensionless term [$d_{50} \theta_n / \tau L$] was proposed to represent the changing soil pore geometry in a contaminated soil block. Here θ_n is the volumetric NAPL content. L is the path length the aqueous

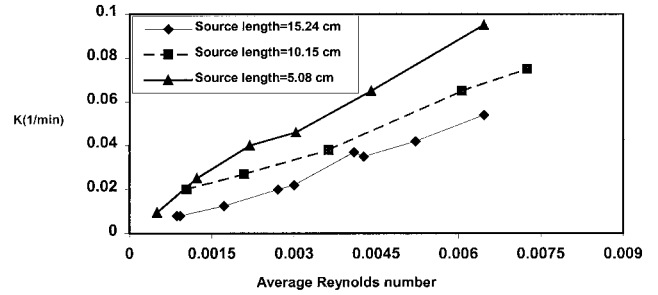


Figure 5. Relation between lumped mass transfer coefficient K averaged over entire source length and Reynolds number (5.08, 10.16, and 15.24 cm long sources).

phase crosses in the contaminated zone (in numerical simulations, L is the length of the contaminated numerical soil block in the flow direction), and τ is the tortuosity of the sand, which corrects for the actual path length taken by the flowing aqueous phase.

The Schmidt number Sc incorporates aqueous phase kinematic viscosity and diffusivity of the LNAPL. Both parameters were assumed to be constant during dissolution experiments conducted in this study. The Reynolds number Re is affected by sand permeability and is expected to change during LNAPL dissolution. On the basis of the principles of these dimensionless numbers we proposed a relation that is expected to govern the mass transfer inside a REV:

$$Sh = a Re^\beta Sc^\alpha \left(\frac{\theta_n d_{50}}{\tau L} \right)^\eta, \quad (5)$$

where Re is the average Reynolds number along the contaminated source zone given by $Re = d_p U'' \gamma^{-1}$, where U'' [$L T^{-1}$] is the actual groundwater velocity. Here a , β , α , and η are fitting parameters. From the proposed model in (5) it is expected that with longer paths of the aqueous phase inside a contaminated zone (L) the average value of the lumped mass transfer coefficient K over the entrapped LNAPL zone will be less. This is because of the decrease in the localized values of k_{la} with distance inside a contaminated zone [Incropera and Dewitt, 1985; Imhoff et al., 1994]. This is consistent with (4) and is supported by the findings of this paper. Figure 5 shows, for the 5.08, 10.16, and 15.24 cm source lengths, the experimental relations between lumped mass transfer rate coefficients over the entire LNAPL source length and the average Reynolds number for the source zone.

Figure 5 shows that for the same Reynolds number, K values over the LNAPL source length increase with decreasing source length. Although the localized value of k_{la} is the same at the upstream end of the three LNAPL zone lengths under the same conditions, this value decreases along the length of the LNAPL zone, and the K value declines.

The Schmidt number Sc represents the ratio of viscous to diffusive forces. Although the Schmidt number was constant throughout our dissolution experiments, it is often included in the mass transfer correlation models [Miller et al., 1990] and is frequently raised to the power 0.33 based on several analytical models and experimental investigations [Miller et al., 1990; Bird, 1960]. Thus, in (5), α was set equal to 0.33.

Table 4. Numerical Model Input Values Used in the Two-Dimensional Dissolution Simulations

	Value
Cell width along rows (Δx), cm	2.5
Cell width along rows inside source zone parallel to flow direction (Δx), cm	0.25, 0.5, 1.0, and 1.25
Cell width along columns (Δy), cm	1.0
Layer thickness (Δz), cm	5.08
Longitudinal matrix dispersivity	0.1
Ratio of transverse to longitudinal dispersivity	0.1
LNAPL source relative permeability	updated spatially with time
Matrix bulk porosity	0.40
LNAPL source saturation, %	22 (updated every time step)
LNAPL source effective porosity	updated spatially with time
Porous media water saturated hydraulic conductivity, cm min^{-1}	7.1
LNAPL partition coefficient in water, $\text{cm}^3 \text{g}^{-1}$	6410
LNAPL density, g cm^{-3}	0.8611
Water density, g cm^{-3}	1.0
Tortuosity	2.0

6. Numerical Tools

Dissolved NAPL introduced into a flow field migrates through aquifers by advection and dispersion. To estimate a lumped mass transfer coefficient K from dissolution data, a mass flux term for NAPL dissolution must be incorporated into the advection-dispersion equation. K values can then be estimated by matching modeled concentration profiles to those obtained from actual experiments.

In order to solve the governing equation of solute transport with a source term introduced to represent entrapped LNAPL a numerical approximation must be developed. The LNAPL zone parameters, such as porosity and hydraulic conductivity, must be modified in the groundwater flow model to reflect the effects of LNAPL entrapment on flow and transport. The groundwater flow and solute transport equations were estimated using MODFLOW [McDonald and Harbaugh, 1988] and MT3D [Zheng, 1990], respectively.

A dissolution package, based on a modified chemical reaction package, was first presented by Okeson [1995] and modified in this work to model dissolution of NAPLs. This package enabled MT3D to handle the necessary computations for rate-limited mass transfer with a linear driving force. The phenomenological model proposed in (5) was added to the dissolution package. The proposed model (equation (5)) determined transient mass transfer rate coefficients over each numerical block on the basis of the transient values of Reynolds number and volumetric LNAPL content during the simulation of the dissolution process.

6.1. NAPL Dissolution and Solute Transport Modeling

Modeling transient flow fields that take into consideration the amount of LNAPL depletion due to dissolving with time allowed accurate simulation of dissolution processes. The modeling analysis of this study was conducted as follows: The modified version of MT3D kept track of the amount of LNAPL dissolved into flowing aqueous phase with time. The impact of LNAPL saturation change on effective porosity and relative permeability was estimated using *Wyllie's* [1962] equation (3). With the new conductivity and porosity data available, MODFLOW was then rerun to obtain new flow fields. The

updated flow fields are then used by MT3D, and the entire process was repeated for every time step until the final target simulation time is reached.

6.2. Regression Analysis

Having integrated MODFLOW and MT3D to work in concert to simulate transient LNAPL dissolution, the problem of assigning mass transfer fitting parameter values to contaminated zones to produce numerical concentration profiles similar to experimental values became an inverse problem that can be solved by least squares regression. The goal of regression was to determine estimates of the unknown fitting parameter values, so that the proposed phenomenological model incorporated into MT3D produced simulated concentration profiles similar to the measured experimental values. This was achieved by minimizing the sum of squared residuals between measured and simulated concentration profiles.

The computer program UCODE [Poeter and Hill, 1998] was used to perform inverse modeling using nonlinear regression to solve for the different fitting parameters. UCODE consists of algorithms programmed in perl, a freeware language designed for text manipulation, and Fortran 90, which performs numerical calculations. Sensitivities of the estimated parameters are calculated by forward or central differences.

The unknown fitting parameters in (5) are a , β , and η . The proposed relation (equation (5)) was applied to each contaminated numerical block. MT3D estimated the values of K over each numerical block on the basis of the transient values of aqueous phase velocity and dissolving volumetric LNAPL content at each time step over all blocks. UCODE was used to minimize the difference between the experimental and numerical breakthrough curves for the three dissolution experiments performed under different groundwater velocities. This was achieved by perturbing the fitting parameter values sequentially using UCODE to determine parameters sensitivities, which are then used by a modified Gauss-Newton iterative scheme to minimize the sum of squared residuals between experimental and numerical breakthrough curves. Numerical simulations of the dissolution experiments were constructed with different numerical block sizes for the tested source lengths under various groundwater velocities. Numerical model input values used for the two-dimensional simulations are shown in Table 4.

Optimized values of a , β , and η , together with their 95% linear confidence intervals, are presented in Table 5. In order to investigate the probability of lumping the different dimensionless numbers presented in (5), correlations between the different fitting parameters were investigated. Correlation was found to be 0.78 between a and η , -0.49 between β and η , and 0.16 between a and β . These low correlation values suggest that the dimensionless groups proposed should not be lumped. Incorporating the optimized fitting parameters gave the following equation:

Table 5. Optimized Values of a , β , and η Together With Their 95% Linear Confidence Intervals

Parameter	Value	95% Linear Confidence Intervals
a	11.34	9.5–13.23
β	0.28	0.24–0.32
η	1.04	1.0–1.07

$$Sh = 11.34 Re^{0.2767} Sc^{0.33} (d_{50}\theta_n/\tau L)^{1.037}. \quad (6)$$

Relations suggested by previous researchers gave an averaged value of the lumped mass transfer rate coefficient K over the length of their laboratory columns as a function of flow parameters and chemical characteristics of the entrapped NAPL [e.g., *Miller et al.*, 1990; *Powers et al.*, 1992, 1994]. These relations, except for *Imhoff et al.* [1994], ignore the fact that the average value of K over a column decreases with the increase in the length of the column. This means that these relations are able to predict a value of K only for contaminated soil blocks with the same lengths as the laboratory columns from which they were estimated. It is not usually feasible or even desirable to model NAPL dissolution in heterogeneous geological media at a spatial resolution equivalent to the scale of laboratory. Instead, the resolution of the numerical model is determined by the much larger scale of grid blocks that discretize the computational domain. Flow and dissolution parameters must then be up-scaled from the laboratory observation to the grid scale. Assigning a value of K from relations estimated from laboratory one-dimensional column observations to the much larger numerical blocks becomes questionable, as it will result in an overestimation of the average value of K over these blocks. In contrast to previous models, this proposed relation has the ability to be up-scaled to different numerical block sizes.

Dissolution experiments performed in one-dimensional laboratory columns developed a dissolution front propagating from upstream to downstream locations [*Imhoff et al.*, 1994]. However, dissolution fronts under multidimensional flow fields are expected to propagate from zones with higher groundwater velocity to zones with lower velocity (this was observed from the numerical simulations of the dissolution experiments). Consequently, the one-dimensional column experiments forced dissolution mechanisms that might have caused errors inherent in the phenomenological models based on one-dimensional flow fields.

7. Comparison With Models Based on One-Dimensional Flow

To evaluate the possible errors that may result from the use of dissolution models developed from one-dimensional experimental data, predictions using models presented by *Powers et al.* [1992] and *Imhoff et al.* [1994] were compared to predictions based on the phenomenological model-suggested (equation

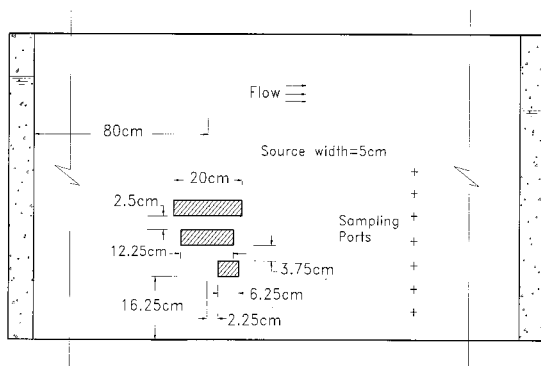


Figure 6. LNAPL sources distribution in the verification experiment.

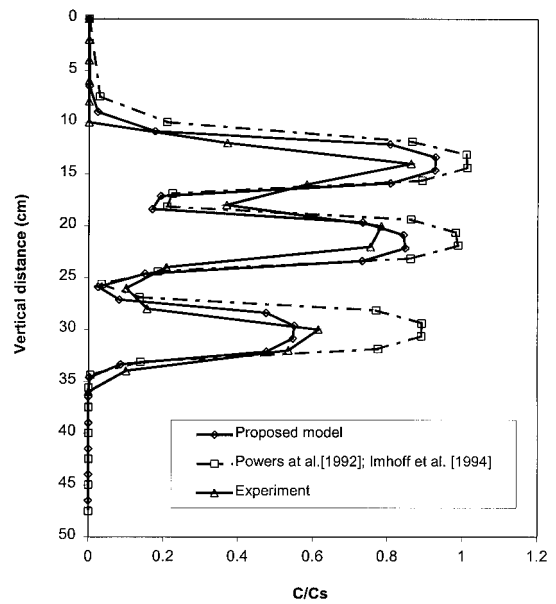


Figure 7. Comparison between vertical concentration profiles for the verification experiment (C_s is the solubility limit of para-xylene in water). *Powers et al.* [1992] and *Imhoff et al.* [1994] results are indistinguishable.

(6)) and experimental data. Each model was incorporated into the modified MT3D code and used to simulate dissolution of three LNAPL sources entrapped altogether in #30 sand (Figure 6). This sand (#30; $d_{50} = 0.049$ cm) is most similar to the sand used by *Imhoff et al.* [1994] ($d_{50} = 0.036$ cm) and is within the range of sands used by *Powers et al.* [1992] ($d_{50} = 0.045$ to 0.12 cm). The contaminated blocks were externally prepared and placed in the intermediate-scale soil flume. LNAPL saturation was found to be 0.22 within all three blocks. Experimental vertical concentration profiles were measured for a discharge of 8.4 mL min^{-1} . Results of the numerical simulations from all models together with the experimental measurements are presented in Figure 7.

As expected, the models of *Powers et al.* [1992] and *Imhoff et al.* [1994] estimated similar dissolution rates, which were higher than actual experimental dissolution rates (Figure 7). This is attributed to the fact that during the column experiments, water is forced through the contaminated zone. This procedure resulted in more dissolved mass introduction to the flowing aqueous phase than under two-dimensional flow fields where the groundwater may bypass contaminated zones due to their lower permeability to the aqueous phase resulting from NAPL entrapment.

8. Summary and Conclusions

In this research, we attempted to understand the effect of flow dimensionality resulting from reduced permeability due to NAPL entrapment on the parameters that quantify mass transfer rates. An experimental method was developed to observe the dissolution of para-xylene trapped at residual saturations under two-dimensional flow fields. Contaminated sources were prepared outside a soil flume under controlled conditions. These sources were then placed within two-dimensional flow fields to conduct dissolution experiments. Evidence of dissolu-

tion fingering was observed from the concentration profile response to different groundwater velocities.

Through numerical modeling of the transient dissolution process together with nonlinear regression analysis, a natural dissolution phenomenological model was proposed. Because of the inclusion of a length factor that takes into account the size of the contaminated zones the proposed model is not constrained to the sizes of the LNAPL zones used in this work and can be up-scaled to different contaminated zone lengths.

The proposed model produced lower quasisteady state dissolution rates when compared to models developed from column experiments. This was attributed to the fact that water was forced through the contaminated zones in the one-dimensional laboratory columns resulting in greater degree of NAPL dissolution compared to the two-dimensional case where flow bypassing can occur. The proposed phenomenological model proved to better predict the dissolved LNAPL concentration profiles than existing models in an independent experiment.

The findings of this study demonstrate the possible errors that can result from the use of parameters obtained from one-dimensional dissolution experiments to make predictions of dissolution behavior in two-dimensional flow systems. This is a first step in the evaluation of such errors that may occur in using characterization data from laboratory experiments to make predictions of NAPL dissolution in three-dimensional field systems.

Notation

- a_{na} Specific interfacial area between NAPL and groundwater for a REV [$L^2 L^{-3}$].
- C Aqueous phase solute concentration in the bulk solution [$M L^{-3}$].
- C_S NAPL solubility limit ($M L^{-3}$).
- d_{50} Mean particle diameter (L).
- D Tube diameter (L).
- D_m Molecular diffusion coefficient for the soluble constituent [$L^2 T^{-1}$].
- J Solute mass flux for a representative elementary volume [$ML^{-3} T^{-1}$].
- k_{la} Average mass transfer coefficient for NAPL-water surface [$L T^{-1}$].
- k_{rw} Relative permeability to flowing aqueous phase.
- K Lumped mass transfer coefficient [T^{-1}].
- L Path length inside a contaminated zone [L].
- Re Reynolds number.
- Sh Sherwood number.
- S Water saturation.
- Sc Schmidt number.
- S_e Effective water saturation.
- S_r Residual water saturation.
- S_n LNAPL saturation.
- τ Tortuosity of sand.
- U Darcy velocity [$L T^{-1}$].
- U'' Actual groundwater velocity [$L T^{-1}$].
- x Linear distance from the column inlet [L].
- γ Kinematic viscosity of water [$L^2 T^{-1}$].
- ε Empirical constant.
- λ Index of the pore size distribution.
- θ_n Initial volumetric NAPL content of the source.
- $\alpha, \beta, \alpha,$ and η Fitting parameters.

Acknowledgments. The authors gratefully acknowledge financial support from USA EPA through Great Plains/Rocky Mountain Hazardous Substances Research Center at Kansas State University.

References

- Bird, R. B., W. E. Stewart, and E. N. Lightfoot, *Transport Phenomena*, John Wiley, New York, 1960.
- Brooks, R. H., and A. T. Corey, Hydraulic properties of porous media, *Hydrol. paper 3*, Colo. State Univ., Ft. Collins, 1964.
- Compos, R., Hydraulic conductivity distribution in a DNAPL entrapped zone in a spatially correlated random field, M.S. thesis, Univ. of Colo., Boulder, 1998.
- Conrad, S. H., E. F. Hagan, and J. L. Wilson, Why are residual saturation of organic liquids different above and below the water table?, paper presented at Conference on Organic Chemicals and Petroleum Hydrocarbons, Natl. Well Water Assoc., Dublin, Ohio, 1987.
- Conrad, S. H., J. L. Wilson, W. Mason, and W. Peplinski, Observing the transport and fate of petroleum hydrocarbons in soils and groundwater using flow visualization techniques, paper presented at Symposium on Environmental Concerns in the Petroleum Industry, Am. Assoc. of Petrol. Geol., Palm Springs, Calif., May 10, 1989.
- Demond, A. H., Capillarity in two-phase liquid flow of organic contaminants in groundwater, Ph.D. thesis, Stanford Univ., Stanford, Calif., 1988.
- Geller, J. T., and J. R. Hunt, Mass transfer from nonaqueous phase organic liquids in water-saturated porous medium, *Water Resour. Res.*, 29, 833–846, 1993.
- Held, R. J., and T. H. Illangasekare, Fingering of dense non-aqueous phase liquids in porous media, 1, Experimental investigation, *Water Resour. Res.*, 31, 1213–1222, 1995.
- Illangasekare, T. H., J. L. Ramsey, K. H. Jensen, and M. Butts, Experimental study of movement and distribution of dense organic contaminants in heterogeneous aquifers, *J. Contam. Hydrol.*, 20, 1–25, 1995a.
- Illangasekare, T. H., E. J. Armbruster, and D. N. Yates, Non-aqueous phase fluids in heterogeneous aquifers: An experimental study, *J. Environ. Eng.*, 121, 571–579, 1995b.
- Imhoff, P. T., and C. T. Miller, Dissolution fingering during the solubilization of nonaqueous phase liquids in saturated porous media, 1, Model predictions, *Water Resour. Res.*, 32, 1919–1928, 1996.
- Imhoff, P. T., P. R. Jaffe, and G. F. Pinder, An experimental study of complete dissolution of a nonaqueous phase liquid in saturated porous media, *Water Resour. Res.*, 30, 307–320, 1994.
- Imhoff, P. T., G. P. Thyrum, and C. T. Miller, Dissolution fingering during the solubilization of nonaqueous phase liquids in saturated porous media, 2, Experimental observations, *Water Resour. Res.*, 32, 1929–1942, 1996.
- Incropera, F. P., and D. P. Dewitt, *Fundamentals of Heat and Mass Transfer*, John Wiley, New York, 1985.
- McDonald, M. G., and A. W. Harbaugh, A modular three-dimensional finite difference groundwater flow model, in *Modeling Techniques, Techniques Water Resour. Invest. U.S. Geol. Surv.*, book 6, 1988.
- Miller, T. C., M. M. Poirier-McNeill, and A. S. Mayer, Dissolution of trapped nonaqueous phase liquids: Mass transfer characteristics, *Water Resour. Res.*, 26, 2783–2796, 1990.
- Okeson, S. J., A study of dissolution of multicomponent nonaqueous phase liquids in a two dimensional flow field and model development, M.S. thesis, Univ. of Colo., Boulder, 1995.
- Pankow, J. F., and J. A. Cherry, *Dense Chlorinated Solvents and Other DNAPLs in Groundwater: History, Behavior and Remediation*, Waterloo, Austin, 1996.
- Pfannkuck, H.-O., Groundwater contamination by crude oil at the Bemidji, Minnesota, research site: U.S. Geological Survey toxic waste-groundwater contamination study, paper presented at Toxic Waste Technical Meeting, U.S. Geol. Surv., Reston, Va., 1984.
- Poeter, E. P., and M. C. Hill, Documentation of UCODE, a computer code for universal inverse modeling, *U.S. Geol. Surv. Water Resour. Invest. Rep.*, 1998.
- Powers, S. E., L. M. Abriola, and W. J. Weber, An experimental investigation of nonaqueous phase liquid dissolution in saturated subsurface systems: Steady state mass transfer rates, *Water Resour. Res.*, 28, 2691–2705, 1992.
- Powers, S. E., L. M. Abriola, and W. J. Weber Jr., An experimental investigation of nonaqueous phase liquid dissolution in saturated

- subsurface systems: Transient mass transfer rates, *Water Resour. Res.*, 30, 321–332, 1994.
- Saripalli, K. P., M. D. Annable, and P. S. C. Rao, Estimation of non-aqueous phase liquid-water interfacial areas in porous media following mobilization by chemical flooding, *Environ. Sci. Technol.*, 31, 3384–3388, 1997.
- Szlag, D. C., Dissolution of trapped waste chemicals, Ph.D. dissertation, Univ. of Colo., Boulder, 1998.
- Wildenschild, D., K. H. Jensen, K. K. Hollenbeck, T. H. Illangasekare, D. Znidarcic, and T. Sonnenborg, A two-stage procedure for determining hydraulic characteristics using syringe pump and outflow observations, *J. Soil Sci. Am.*, 61(2), 347–359, 1997.
- Wyllie, M. R. J., *Relative Permeability in Petroleum Production Handbook*, vol. II, *Reservoir Engineering*, McGraw-Hill, New York, 1962.
- Zheng, C., MT3D: A modular three-dimensional transport model for simulation of advection, dispersion, and chemical reactions of contaminants in groundwater systems, *Rep. 74280*, U.S. EPA Roberts S. Kerr Environ. Res. Lab., Ada, Okla., 1990.
- Znidarcic, D., T. H. Illangasekare, and M. Manna, Laboratory testing and parameter estimation for two-phase flow, paper presented at Conference in Geotechnical Engineering, Am. Soc. of Civ. Eng., New York, 1991.
-
- T. H. Illangasekare and T. Saba, Division of Environmental Sciences and Engineering, Colorado School of Mines, Golden, CO 80401. (tillanga@mines.edu; saba@bechtel.colorado.edu)
- (Received April 16, 1998; revised October 29, 1999; accepted October 29, 1999.)

